

# Intercomparison of snow density measurements: bias, precision and vertical resolution

**M. Proksch<sup>1,2</sup>, N. Rutter<sup>3</sup>, C. Fierz<sup>1</sup>, and M. Schneebeli<sup>1</sup>**

<sup>1</sup>WSL Institute for Snow and Avalanche Research SLF, Flüelastrasse 11,  
7260 Davos Dorf, Switzerland

<sup>2</sup>Institute of Meteorology and Geophysics, University of Innsbruck, Innrain 52,  
6020 Innsbruck, Austria

<sup>3</sup>Department of Geography, Northumbria University, Newcastle upon Tyne, UK

Correspondence to: M. Schneebeli (schneebeli@slf.ch)

## Abstract

Density is a fundamental property of porous media such as snow. A wide range of snow properties and physical processes are linked to density, but few studies have addressed the uncertainty in snow density measurements. No study has yet quantitatively considered the recent advances in snow measurement methods such as micro-computed tomography ( $\mu$ CT) in alpine snow. During the MicroSnow Davos 2014 workshop different approaches to measure snow density were applied in a controlled laboratory environment and in the field. Overall, the agreement between  $\mu$ CT and gravimetric methods (density cutters) was 5 to 9%, with a bias of  $-5$  to  $2\%$ , expressed as percentage of the mean  $\mu$ CT density. In the field, the density cutters tend to overestimate ( $1$  to  $6\%$ ) densities below and underestimate ( $1$  to  $6\%$ ) densities above a cutter-type dependent threshold that fell between  $296$  to  $350$   $\text{kg m}^{-3}$ , respectively. Using the mean per layer of all measurement methods applied in the field ( $\mu$ CT, box, wedge and cylinder cutter) and ignoring ice layers, the variation of layer density between the methods was  $2$  to  $5\%$  with a bias of  $-1$  to  $1\%$ . In general, our result suggests that snow densities measured by different methods agree within  $9\%$ . However, the density profiles resolved by the measurement methods differed considerably. In particular, the millimeter scale density variations revealed by the high resolution  $\mu$ CT contrasted the thick layers with sharp boundaries introduced by the observer. In this respect, the unresolved variation, i.e. the density variation within a layer, which is lost by sampling with lower resolution or layer aggregation, is critical when snow density measurements are used as boundary or initial conditions in numerical simulations.

## 1 Introduction

Density is a fundamental property of porous media (Torquato, 2002) such as snow. It plays a key role for a wide range of applications and almost all of them require density values. Snow hydrology (Pulliainen and Hallikainen, 2001) and climatology (Derksen and Brown, 2012) based on microwave remote sensing require snow density, as it is directly linked to

the relative permittivity of dry snow (Tiuri et al., 1984; Mätzler, 1996). Light transmission and the extinction coefficient of snow depend on density, and as such density affects the optical properties of snow (Kokhanovsky and Zege, 2004; Gergely et al., 2010). The biological and photochemical activities of snow are related to snow density (Domine et al., 2008). Further, snow mechanical parameters are linked to density (Schneebeli and Johnson, 1998; Wang and Baker, 2013) and snowpack stability depends on vertical density variations (Schweizer et al., 2011).


In addition, parametrization of snow physical properties such as permeability (Shimizu, 1970; Calonne et al., 2012; Zermatten et al., 2014), thermal conductivity (Adams and Sato, 1993; Sturm et al., 1997; Calonne et al., 2011) are linked to density. Snow models like SNTHERM (Jordan, 1991), CROCUS (Brun et al., 1989) and SNOWPACK (Lehning et al., 2002) adopted density for the parametrizations of such properties as well, and models describing ventilation and air flow (Albert, 1996), isotopic content in polar snow (Neumann and Waddington, 2004; Town et al., 2008) or drifting snow (Lenaerts et al., 2012) also require density.


As important as density is, there are many properties, notably albedo (Flanner and Zender, 2006; Domine et al., 2007), where higher order geometric descriptors like specific surface area (SSA) or anisotropy are necessary, as Löwe et al. (2013) showed for thermal conductivity. As such, a precise measurement of snow density and its variation in horizontal and vertical direction is of major importance to better understand and model a wide range of snow physical processes. Despite its relevance, few studies quantified so far the differences between the methods to measure snow density. Indeed several studies focused on firn and ice density, but those were mostly limited to firn and ice, i.e. density ranges ( $> 500 \text{ kg m}^{-3}$ ) larger than the one typically found in alpine snow ( $50 - 400 \text{ kg m}^{-3}$ ). Carroll (1977) compared tube and box type density cutters and reported no significant difference between the two cutter types (although there was a tendency for inexperienced users to overestimate the density of light snow and depth hoar by 6 and 4 %, respectively). Conger and McClung (2009) compared box, wedge and cylinder type density cutters and reported a variation of up to 11 % between the three cutter types. Both studies compared only mea-

surement methods of the same type, the direct gravimetric measurement of snow samples with a well defined volume.

However, there are more methods available to measure snow density besides the gravimetric approach: stereology (Matzl and Schneebeli, 2010) determines density on the millimeter scale in vertical sections; micro-computed tomography ( $\mu$ CT, (Schneebeli and Sokratov, 2004; Lundy et al., 2002)) allows the reconstruction of the complete 3-D microstructure of small (centimeter) snow samples and calculation of the snow density with a resolution of up to 1 mm. In addition, high resolution penetrometry (SMP, Schneebeli and Johnson, 1998) was recently shown to be suited to derive snow density (Proksch et al., 2015). Dielectric devices were developed to measure snow density, as the dielectric permittivity of dry snow is not strongly affected by other structural properties at certain frequencies (Denoth et al., 1984; Tiuri and Sihvola, 1986; Kendra et al., 1994; Mätzler, 1996). Neutron absorption (Kane, 1969; Morris and Cooper, 2003) was in particular used to measure density inside a firn or ice bore hole. Another method in development is diffuse near-infrared transmission (NIT, Gergely et al., 2010) that allows to derive the density of snow in macroscopic vertical sections with millimeter resolution in the horizontal and vertical direction.

Advantages of these approaches are substantial compared to the gravimetric measurement systems. The vertical resolution of the  $\mu$ CT, SMP and NIT in the millimeter range is clearly a significant improvement to the centimeter resolution of the gravimetric systems. The impact of measurement resolution was in particular demonstrated by Harper and Bradford (2003), who showed that the identification of stratigraphy is a function of a tool's sensitivity to vertical contrast. Hawley et al. (2008) in addition highlighted the smoothing of the density profile of an ice core for instruments with larger vertical measurement length. In terms of measurement time, the SMP is more time efficient as excavation of a snow pit is not necessary. Vertical profiles of snow density through repeated measurements with the SMP allow the investigation of the spatial variability of snow density. Proksch et al. (2015) demonstrated the use of the SMP to reveal spatial density variations in an Antarctic snow profile. Although spatially varying density is a known problem for a broad range of applica-

tions (e.g. Rutt  et al., 2014), an intercomparison of the ability of the different methods to resolve vertical density variations was beyond the scope of this study.

Several studies have compared different methods to measure density, but were mostly limited to firn and ice, i.e. a density range ( $> 500 \text{ kg m}^{-3}$ ) larger than the one typically found in alpine snow (50 - 350   $\text{kg m}^{-3}$ ). Freitag et al. (2004) compared firn densities measured by  $\mu\text{CT}$  with those measured by gamma-absorption for three sections of a firn core, each approx. 60 cm long. The authors report a deviation of less than 1 % for both methods in the density range from 640 - 733  $\text{kg m}^{-3}$ , but also qualitatively higher values for the  $\mu\text{CT}$  in the range 460 - 550  $\text{kg m}^{-3}$  and lower values for the  $\mu\text{CT}$  for densities above 733  $\text{kg m}^{-3}$ . However, no results are reported for densities below 460  $\text{kg m}^{-3}$ , which were in evidence at the workshop. Kawamura (1990) reported good agreement between CT and the hydrostatic method to determine the density of ice cores. Hawley et al. (2008) compared neutron probing, dielectric profiling, optical stratigraphy of the core and gravimetric measurements on an 11 m firn and ice core from Kongsvegen, Svalbard. The authors reported a smoothing of thin ice layers in particular for the neutron probe due too its large detector size of 13.5 cm, but also for the dielectric device due too its finite sampling volume, where the authors estimated a sensing length of approx. 4 cm. Other problems related to the gravimetric and dielectric measurements were mentioned with respect to collecting cores (accurate measurement of borehole diameter, depth registration, core breaks, poor core quality or melting of cores during shipping) or loose snow at the surface of the bore hole.

Studies which quantitatively focus on snow rather than firn or ice are rarely available. A study which compared density measured by CT and by weighing samples of sieved was presented by Lundy et al. (2002). The authors reported qualitatively a good agreement between both methods for their 4 investigated samples, however, none of the three density cutters used in our study was used. Dielectric devices were also compared to gravimetric measurements. Kendra et al. (1994) found an RMSE of their snow probe of  $\pm 50 \text{ kg m}^{-3}$  compared to gravimetric measurements only in a qualitative way, whereas a RMSE of maximum 9 % (29.7  $\text{kg m}^{-3}$ ; lab data, box cutter to  $\mu\text{CT}$ ) was found for our data.

Although the non-gravimetric approaches have advantages compared to the simple density cutters, there are major drawbacks to be mentioned. Besides cost and evaluation time, the technical simplicity, robustness, portability and ease of use of the density cutters remain attractive characteristics. However, for a wide range of applications, users need the higher resolution and efficiency of technologically more sophisticated measurement methods.

Besides this, many applications exist that (to date) do not require high resolution profiles. For instance, microwave remote sensing applications often use 1 or 2 layer snow models in operational retrievals. Consequently, the scope of this paper is to show how high resolution measurements, simplified to coarser vertical resolution, compare to traditional profiles, i.e. to quantify how millimeter scale profiles aggregate back to coarser vertical resolutions.

This paper focuses on density data measured during the MicroSnow Davos workshop held in March 2014, i.e. different types of density cutters as well as  $\mu$ CT measurements. The MicroSnow Davos workshop aimed to quantify the differences between available snow measurement methods, motivated by the progress in the development of new measurement methods in the recent years. SMP derived densities were discarded due to the use of a new version of the instrument, for which the calibration of Proksch et al. (2015) was not applicable. The main objective of this paper is to intercompare the available measurement methods (box cutter, wedge cutter, density per layer and  $\mu$ CT) and to assess the error and the variability between methods as well as their respective measurement resolution. The paper is organized as follows: Sect. 2 introduces the measurement methods and Sect. 2.4 the available data from the field and the laboratory. Section 3 summarizes the results, which are discussed in Sect. 4. Section 5 concludes our findings.

## 2 Methods

### 2.1 Samples and stratigraphic layers

All instruments provided density profiles with different vertical resolution. For clarity, we discriminate between *layer* and *sample*. A stratigraphic *layer* is a certain stratum with similar

properties (e.g. microstructure, density, snow hardness, liquid water content, snow temperature, impurities) in the snowpack as defined in Fierz et al. (2009). Layers thus represent a stratigraphic arrangement of the snowpack, as classified by an observer, with heights ranging from a few millimeters to several decimeters. However, the determination of layer boundaries in the snowpack depends on the observer and different observers will identify different layering. In addition to layers, a *sample* is a specific volume extracted from the snowpack in order to measure a certain property. Sampling can be performed independently of the stratigraphic layering and results in a constant vertical resolution, which is given by the vertical size of the sample; the resolution can be both enhanced or reduced by overlapping or spacing samples, respectively.

In this study, the cylinder cutter was used to measure the density per layer, after the layers were determined following Fierz et al. (2009). All other method were used to measure the density per sample. As such, the cylinder cutter provided a density profile with varying vertical resolution, based on the thickness of the layers, contrasted by box and wedge cutter, as well as  $\mu$ CT, which were operated with constant vertical resolution. The high resolution  $\mu$ CT also belongs to the sample category, as it is operated with a constant vertical resolution.

## 2.2 Instruments


The following section gives, together with Table 1, an overview of the instruments and methods which were used to measure snow density during MicroSnow Davos workshop in 2014.

### 2.2.1 Micro-Computed Tomography



Micro-Computed Tomography ( $\mu$ CT) (Schneebeli and Sokratov, 2004) allows the full 3-D microstructure of snow to be reconstructed.  $\mu$ CT measurements of snow result in a gray scale, which was filtered using a Gaussian filter ( $\sigma = 1$  voxel, support = 1 voxel, following (Kerbrat et al., 2008)) and then segmented into a binary image. The threshold for segmentation was constant for each sample and determined visually. After segmentation, the binary image contains the full microstructure and allows to derive the volume fraction  $\phi_i$  of the

snow sample, which is then related to the mass density  $\rho$  of snow by  $\rho = \rho_{\text{ice}} \phi_i$  in terms of the density  $\rho_{\text{ice}} = 917 \text{ kgm}^{-3}$  of ice.

### 2.2.2 Density cutters

Density cutters provide a gravimetric measurement, where the density is calculated by weighing a defined snow volume, which is extracted from the snow by using a cylinder, wedge or box type cutter. Figure 1 shows the three different types of cutters which were used during the workshop: (a) a  $100 \text{ cm}^3$  box cutter,  $6 \text{ cm} \times 3 \text{ cm} \times 5.5 \text{ cm}$  originating from the Institute of Low Temperature Science, Japan, now known as Taylor-LaChapelle density cutter, manufactured by snowhydro (<http://www.snowhydro.com/products/column4.html>) and WSL-SLF, (b) a  $100 \text{ cm}^3$  cylinder cutter,  $3.72 \text{ cm}$  inner diameter and  $9.2 \text{ cm}$  in height, constructed from an aluminum cylinder with one end sharpened to cut cleanly through the snow and (c) a  $1000 \text{ cm}^3$  wedge cutter,  $20 \text{ cm} \times 10 \text{ cm} \times 10 \text{ cm}$  manufactured by snowmetrics (<http://snowmetrics.com/shop/rip-1-cutter-1000-cc/>). In addition, a cylinder of inner diameter  $9.44 \text{ cm}$  and length  $55 \text{ cm}$  (also ically inserted into the snow) was used to determine the bulk density.

### 2.2.3 Traditional stratigraphy and density per layer

After the stratigraphic arrangement of the snowpack was identified (see Sect. 2.1), density measurements were made within each layer. The  $100 \text{ cm}^3$  cylinder cutter inserted vertically down through the snow to a pre-placed crystal screen (see also Conger and McClung, 2009) was used to extract snow samples with  stratigraphically defined layers. Samples were weighed using an ACCULAB Pocket Pro 2003B  with a resolution and nominal accuracy of  $\pm 0.1 \text{ g}$ . Each density measurement is repeated twice and the average of both samples taken as either layer or sub-layer density. The density of layers, the height of which are less than the cylinder length, can be calculated using the ratio of the layer height and the cylinder length. However, in general layers thinner than about  $2 \text{ cm}$  are aggregated to adjacent upper or lower layers and cannot be resolved with regard to density except when the hardness



of the layer itself or of an adjacent layer is greater than a hand hardness index of 3 (i.e. 1 finger, see Fierz et al., 2009). In that case, a sample may be cut out of the snow and by measuring its dimensions and weight its density can be estimated. If the sample contains two layers, the softer one may then be gently scrapped away to allow for determining the density of the harder layer. Using both measurements yields the density of the softer layer. Such measurements are prone to large errors ( $\geq 10\%$ ) even by a skilled observer. Three melt-freeze crusts or ice lenses were determined in this manner.

Conversely, where vertical layer thickness was larger than the cylinder length, seamless sampling down the layer was required to determine its mean density. In that case, densities at sub-layer scale may be obtained within a layer. Finally, depth averaging the layer densities over the full profile yields the Snow Water Equivalent (SWE) of the snowpack.

The density per layer or traditional stratigraphy is termed "cylinder cutter" hereafter, as only the cylinder cutter was used in this study to determine the density per layer. All other devices (box and wedge cutter,  $\mu$ CT) were operated without considering layering or stratigraphy of the snowpack, i.e. with constant vertical resolution (see also Section 2.1).

### 2.3 Comparing measurements with different vertical resolutions

Intercomparison of measurements with different vertical resolutions followed three different approaches:

- a. The mean density over the full depth of a profile is related to the snow water equivalent (SWE) of the snowpack. However, unlike SWE, it can be compared independently of the actual snow depth. The comparison of this value showed whether the means of all methods were consistent with each other.
- b. The high resolution  $\mu$ CT profile was averaged to match the vertical resolution of the three different cutters, as solely the  $\mu$ CT provided a high enough resolution (1.08 mm) to be averaged to the resolution of all other gravimetric methods. This allowed comparison of each method with its original resolution, without any averaging (besides the  $\mu$ CT which was used as a reference). A linear regression was then calculated for each

comparison. The point of intersection between the linear regression line and the 1 : 1 line was defined as threshold between over- and under-estimation with respect to the  $\mu$ CT density.

- c. To facilitate a more objective comparison where none of the instruments was set as reference, all measurements were depth-averaged to the same coarse vertical layer resolution of the cylinder cutter. Similar to Conger and McClung (2009), the mean density per layer of all instruments was assumed to be the accepted reference value of the layer density, and all instruments were compared against this reference value. As the vertical resolution of the box and wedge type cutters did not match the traditional layers, a depth weighted layer average was applied.

## 2.4 Data collection

### 2.4.1 Lab measurements

Thirteen snow blocks of 40 cm x 40 cm in area and between 10 and 36 cm in height were used in this study. The major grain types of the snow blocks were facets (n=7), rounded grains (n=3) and depth hoar (n=3), as classified according to Fierz et al. (2009). All blocks were measured using the  $\mu$ CT and the 100 cm<sup>3</sup> box type density cutter in the laboratory, at a constant air temperature of  $-10^{\circ}\text{C}$ .  $\mu$ CT samples were taken from depths between 2.9 and 6.8 cm from the surface of the block. Up to three samples were taken per block; two samples were extracted using a 35 mm diameter sample holder, and one using a 20 mm diameter sample holder. The samples in the 35 mm sample holder were scanned with a resolution of 0.018 mm, within the scanned volume of 15<sup>3</sup> mm<sup>3</sup>, whereas the samples in the 20 mm sample holder were scanned with a resolution of 0.010 mm within the scanned volume of 10<sup>3</sup> mm<sup>3</sup>; the representative cubic volume to derive density from  $\mu$ CT measurements is around 1.25<sup>3</sup> mm<sup>3</sup> (Kaempfer et al., 2005).

Continuous box cutter measurements were performed from the snow surface to the bottom of the snow block with a vertical resolution of 3 cm leading to a maximum of 8 measurements per block. For comparison with  $\mu$ CT densities, the upper most three cutter measure-

ments (0–9 cm snow depth) were analyzed, to avoid any misalignment with the location of the  $\mu$ CT measurements. An overview of the lab measurements is given in Table 2.

### 2.4.2 Field measurements

The field site of the workshop was a tennis court in St. Moritz (46.4757° N, 9.8224° E) surrounded by forest, fenced, wind sheltered and flat, and as such showed a very homogeneous natural snowpack. For instance, wedge cutter measurements, where two profiles were performed within 20 cm horizontal distance, showed a mean difference of 7 kg m<sup>-3</sup> or 2 % of the mean wedge cutter density. All density measurements were performed within less than 3 m horizontal distance. Field measurements were made on 11 and 12 March 2014 (Table 3). Warm temperatures caused surface melt after the measurements during the first day, leading to densification of the upper-most layers and to more pronounced crust and ice layers on the second day. Measurements were made between 04:00–09:00 each day, while the snowpack was still dry.

To analyze a profile completely from top to bottom by means of  $\mu$ CT, five blocks of 20 cm × 20 cm × 30 cm were extracted from the snowpack on 11 March 2014. Snow blocks were quickly transported to the lab and each block was sampled using 35 mm diameter sample holders, leading to a total of 18  $\mu$ CT samples for the whole vertical profile. Each sample was scanned with a resolution of 0.018 mm within a scanned volume of 10.8 mm × 10.8 mm × 2.16 mm. Scans were performed with a vertical overlap of 50 %. The density was then resampled in a window of 1.08 mm depth. Field  $\mu$ CT samples were evaluated using the classic segmentation approach (Sect. 2.2.1). Three types of density cutters (Sect. 2.2.2) were used in the field. Measurements using the cylinder cutter (densities per layer) and wedge cutter were made on 11 March and box cutter measurements were made on 12 March. All measurements were performed within two meters horizontal distance.

### 3 Results

#### 3.1 Lab results

Box cutter and  $\mu$ CT measurements agreed within 8 % (Fig. 2, Table 4). The box cutter measurements showed slightly higher densities, with a bias of 5 %, expressed as percentage of the mean of  $\mu$ CT density. The coefficient of determination  $R^2$  was 0.90, significant at the 1 % level.

#### 3.2 Field results

The density profiles of all instruments are shown in Fig. 3. Three types of comparisons (Sect. 2.3) were performed, all excluding ice layers. For comparison a), the bulk densities derived from each method were compared. In addition a cylinder of inner diameter 9.44 cm and length 55 cm (Sect 2.2.3) was used, where the sampling was performed similarly to the mean density of a thick layer (see Sect. 2.2.3), yielding a bulk density of  $325 \text{ kg m}^{-3}$ . The bulk density calculated from the cylinder cutter was  $332 \text{ kg m}^{-3}$ , from the box cutter  $344 \text{ kg m}^{-3}$ , from the wedge cutter  $316 \text{ kg m}^{-3}$ , and from the  $\mu$ CT  $323 \text{ kg m}^{-3}$ .

For comparison b), all methods were compared to the  $\mu$ CT density profile. For this reason, the high resolution  $\mu$ CT profile was averaged to match the vertical resolutions of the box and wedge type density cutters, as well as the layer heights of the traditional stratigraphic profile. Box and wedge cutter and densities per layer agreed with the  $\mu$ CT within 7, 9 and 5 % with a bias of  $-1$ , 2 and  $-1$  %, respectively, expressed as percentage of the mean  $\mu$ CT density (Fig. 4, Table 4). Box cutter, wedge cutter and densities per layer (Sect. 2.2.3) overestimated low densities (4, 6 and 1 %, respectively) and underestimated high densities (2, 6 and 1 %, respectively) with respect to the  $\mu$ CT densities. The threshold to discriminate between low and high densities, and over- and under-estimation, was 350, 310 and  $296 \text{ kg m}^{-3}$  for box cutter, wedge cutter and densities by layer, respectively. Further details are given in Table 5.

For comparison c) and to facilitate a more objective comparison, all measurements were averaged to the same vertical resolution, i.e. to match the traditional stratigraphic layers. The mean density per layer of all instruments was then set as reference. With respect to this reference, the different methods agreed within 2 to 5 % (Fig. 5, Table 6), the bias was

5 between -1 and 1 % and  $R^2 = 0.99$  for all instruments, significant at the 1 % level. When ice layers were not excluded, the different instruments agreed within 12 to 35 % with the mean layer density, with a bias of -10 to 12 % (Table 6).

### 3.3 Unresolved variation: density variation within a layer

Figure 6 shows the  $\mu$ CT density which was subsequently averaged to a comparable vertical resolution as the cutters. The high degree of detail in the  $\mu$ CT density profile vanishes in this case. Figure 7 shows the unresolved variation, i.e. the density variation within a layer. It was calculated as standard deviation of the  $\mu$ CT density within a certain vertical distance. For instance, for the 100 cm<sup>3</sup> box cutter which had a vertical resolution of 3 cm, the  $\mu$ CT profile was averaged to 3 cm vertical resolution and the standard deviation for each

15 3 cm window was derived. The mean of all these standard deviations was then defined as unresolved variance (in this case for the 100 cm<sup>3</sup> box cutter with respect to the  $\mu$ CT density). The arrows in Figure 7 indicate the density variation which is lost when sampling with the box and wedge cutter (3 and 10 cm height, respectively). For the 100 cm<sup>3</sup> box cutter the unresolved variation is  $17 \pm 13 \text{ kg m}^{-3}$  and for the 1000 cm<sup>3</sup> wedge cutter  $23 \pm 11 \text{ kg m}^{-3}$ .

20 If the  $\mu$ CT profile is averaged to match the layers of the traditional profile, the unresolved variation increases to  $25 \pm 16 \text{ kg m}^{-3}$ .

## 4 Discussion

### 4.1 Laboratory results

The higher density values from the 100 cm<sup>3</sup> box cutter compared to the  $\mu$ CT (Fig. 2) corroborate the overestimation reported by Carroll (1977) for this cutter type. However, Carroll

(1977) found this for light snow (i.e. where the snow was compacted) depth hoar (i.e. where single crystals broke at the edge of the cutter and filled the void space around the cutter). Neither type of snow was very prominently present in the snow blocks used in the laboratory.

## 4.2 Field results

The bulk density Sect. 2.3, comparison a) ranged from 316 to 344 kg m<sup>-3</sup>, with a coefficient of variation of 3 %. Assuming the mean of all bulk densities, which was 328 kg m<sup>-3</sup>, as accepted reference bulk density value, the wedge cutter, the  $\mu$ CT and the bulk density from the 55 cm cylinder (as described in Sect. 3.2) underestimated the mean bulk density by 4, 3 and 1 %, respectively. The cylinder cutter and the box cutter overestimated the mean bulk density by 2 and 5 %, respectively. The oversampling of the box cutter is partly attributed to the fact that the box cutter measurements were made on the second day, after melt occurred in the upper layers during the first day and a slight settling of the snowpack, with a decrease in snow height from 140 cm on the first day to 136 cm on the second day. Underestimation by the wedge cutter was already observed by Conger and McClung (2009), due to displacement of the cutter as the cutting plate neared the thin leading edge of the wedge.

The intercomparison (Sect. 2.3, comparison b) shows similar results for the blocks in the laboratory as the measurements in the field. The cutter and  $\mu$ CT measurements agreed within 5 to 9 % (8 % in the lab) and showed a bias of -1 to 2 % (-4 % in the lab). However, the three measurement methods overestimated low densities (1 to 6 %) and underestimated high densities (1 to 6 %) with respect to the  $\mu$ CT density (Fig. 4 and Table 5). In contrast, lab data showed slightly higher cutter densities in general (Sect. 3.1) and no underestimation for the higher densities was found in the lab. This was caused by storing the blocks up to eight weeks at constant temperature. During the isothermal storage the thickness of the ice matrix increased at nearly constant pore space (Kaempfer and Schneebeli, 2007). The snow blocks were therefore less fragile, and it was easier to take intact, unbroken samples in the lab.

Carroll (1977) also reported an overestimation of light snow densities by 6 % using different density cutters. The authors found this overestimation occurred with inexperienced users, which was not the case at the Davos workshop, where each instrument was operated by the same expert user. Thus the overestimation was attributed to the device itself, in particular to the compaction of light snow while inserting the cutter into the snowpack. The largest bias was found for the wedge cutter (6 %), which was attributed to the design of the cutter: because 75 % of the measured volume of the wedge cutter is in the lower half of the cutter (Conger and McClung, 2009), the increasing density with depth causes a systematic oversampling of denser snow. For higher densities, Carroll (1977) reported also an overestimation. In contrast, higher densities were underestimated at the workshop, caused by loosing parts of the sample in very fragile facets and depth hoar, which appear in the lower part of the snowpack in the field. This underestimation is largest for the wedge cutter, due to the displacement of the cutter while closing it with the cutting plate (Conger and McClung, 2009).

The comparison of all instruments with the stratigraphic layers (Sect. 2.3, comparison c) compares the aggregated mean and variation. Ignoring ice lenses, the variation between  $\mu$ CT and cutter densities was within 2 to 5 % with a bias of  $-1$  to 1 % (Table 5) with respect to the mean layer density. Those values are lower than comparison (b), setting the  $\mu$ CT as reference. A higher variation occurs in a comparison of single instruments with each other than with the mean of all instruments.

The effect of density variation in the range presented above is illustrated with respect to the calculation of thermal conductivity and snow stability. Assuming a density of  $300 \text{ kg m}^{-3}$  and a variation of 10% or  $30 \text{ kg m}^{-3}$ . The uncertainty in thermal conductivity based on the parametrization by Calonne et al. (2011) would be 21% (thermal conductivity at  $300 \text{ kg m}^{-3}$ :  $0.212 \text{ W K}^{-1}\text{m}^{-1}$ ; error  $0.045 \text{ W K}^{-1}\text{m}^{-1}$ ), due to the almost quadratic dependence between thermal conductivity and density. However, the critical cutting length, a measure for snow instability, has an almost linear dependence. It increases only by 9% (from 0.53 cm to 0.59 cm), if the density of the snow slab on top of the weak layer is increased by 10 % from  $300 \text{ kg m}^{-3}$  to  $330 \text{ kg m}^{-3}$  following the procedure described in Reuter et al.

(2015) (slab height 60 cm, weak layer fracture energy  $0.5 \text{ J m}^{-2}$ , elastic modulus of the snow slab derived from Scapozza and Bartelt (2003), slope angle  $0^\circ$ ).

In addition possible uncertainties introduced by the  $\mu\text{CT}$  should be addressed. The main uncertainty of the  $\mu\text{CT}$  density lies in the segmentation of grey-scale images into binary images. In this study, the threshold for image segmentation was visually determined by a trained operator. Both visual and automated threshold determination (e.g. Kerbrat et al. (2008)) are based on the same principle, finding the minimum between the ice and air peak in the grey scale histogram, but a trained operator is able to compensate for the disadvantages of automated threshold selection e.g. at uni-modal histograms for snow samples with high SSA. However, no error estimate is available for the visual technique, but Hagenmuller et al. (2013) reported similar density values for an automated threshold segmentation, gravimetric measurements and an energy based segmentation developed by these authors. The authors further noted that both segmentation techniques produce basically identical results, which gives also confidence for the visual threshold based segmentation used in this study, as the principle behind both techniques is the same. For the sensitivity of the threshold selection, Hagenmuller et al. (2013) reported that the density of a snow sample (gravimetric density of  $280 \text{ kg m}^{-3}$ ,  $\mu\text{CT}$  determined SSA of  $8.0 \text{ mm}^{-1}$ ) the dilation of a pixel would increase the density from  $278 \text{ kg m}^{-3}$  to  $294 \text{ kg m}^{-3}$  which is on the order of 5 %. In general, the strength of the  $\mu\text{CT}$  derived density is the precise information of the density evolution enabled by the sub-millimeter scale resolution of the  $\mu\text{CT}$ ; the absolute density is more sensitive to the segmentation process. As such, the analysis of field data presented in this study, which focused on density evolution with depth, is expected to be fairly insensitive on the  $\mu\text{CT}$  segmentation process, whereas the bias values are more sensitive to the segmentation. Providing  $\mu\text{CT}$  error values would, however, require extensive re-segmentation of  $\mu\text{CT}$  samples, which is beyond the scope of this study.

#### 4.2.1 Representation of the stratigraphy by the density measurements

As the stratigraphy is defined by several properties, density alone is always an insufficient parameter for the traditional stratigraphy. Here we demonstrate that the traditional stratigraphy



phy often shows much sharper boundaries than the density measurements would indicate (Fig. 3). Traditional stratigraphy showed a highly detailed representation of specific types of density variations such as ice layers in the upper part of the profile, contrasted by a very coarse representation in the lower part; only one single layer was determined from 90 to 130 cm depth (Fig. 8). Nevertheless, three sub-layers could be identified within this layer, the density difference of which could not be explained by inter-sample variability ( $4.2 \text{ kg m}^{-3}$  or 1.1 %). While the sub-layer densities of 382, 400, and  $418 \text{ kg m}^{-3}$  from top to bottom reproduced the trend of both box and wedge cutter measurements, the cylinder cutter did not represent these variations. Further, the wedge cutter did not represent the variations measured by the box cutter, and the box cutter did not represent the variations measured by the  $\mu\text{CT}$ . Figure 8 illustrates this fact: on the one hand, layer boundaries, which were defined following the traditional stratigraphic approach (Fierz et al., 2009), appeared less distinct in the  $\mu\text{CT}$ , and on the other hand, the higher resolution methods resolved a high degree of variability within a layer. We would like to point out here that sharp boundaries, as introduced by the observer, compared to the very smooth development of the high resolution measurements, may introduce a significant bias in numerical simulations, when observed snow profiles are used as initial conditions. The effect of different stratigraphic representations on microwave emission modeling was unambiguously demonstrated. Durand et al. (2011) estimated the error in retrieved snow depth from passive microwave simulations up to 50 % due to neglecting stratigraphy. Rutter et al. (2014) showed that the bias of a three layer representation of a tundra snowpack with respect to microwave emission was half of the bias for a single layer representation. For the validation of snow cover models, Monti et al. (2012) mentioned the higher number of simulated layers than observed ones to be critical.

The fact that the higher resolution methods resolved a higher degree of density variation is closely related to the measurement volume of the different instruments. For instance, the measurement volume of the  $\mu\text{CT}$  ( $15^3 \text{ mm}^3 = 3375 \text{ mm}^3 = 3.375 \text{ cm}^3$ ) is around 3 % the measurement volume of the  $100 \text{ cm}^3$  box density cutter. A larger measurement volume is immutably connected to a smoothing of the measured density profile, as thin layers are av-

eraged within the measurement volume. This explains the lower variability of the box cutter density profile, compared to the high frequency density variations resolved by the  $\mu$ CT, and is also true for the lower variability of the 1000 cm<sup>3</sup> wedge cutter compared to the box cutter. As the measurement volume of the  $\mu$ CT was sufficiently large to be representative (1.25<sup>3</sup> mm<sup>3</sup> = 1.95 mm<sup>3</sup>, Kaempfer et al. (2005), Section 2.4.1), these high frequency density fluctuations are not an artefact of a small measurement volume.

#### 4.2.2 Ice layers

The spatially discontinuous near-surface ice layers decreased the agreement between different field measurements (Table 5). Box and wedge cutters did not fully resolve the ice layers in the field, in contrast to the stratigraphic method.

Ice layer densities were determined by careful measurement of an extracted ice layer. Uncertainties remain in measurements of ice layer densities using this technique, largely due to the triaxial volume measurement of an irregular-shaped ice sample in combination with the precision of the in-situ mass measurement ( $\pm 0.1$ g) relative to the mass of the sample. When using box and wedge cutter, ice layers represented only a small part of the sampled snow volume. The box cutter showed two distinct density peaks, but with values of 409 and 405 kg m<sup>-3</sup> these measurements were lower than the layer densities of 567 and 760 kg m<sup>-3</sup> for the upper and lower ice layers, respectively (Fig. 3). In contrast, the wedge cutter did not show any significant density peak. The perceived lack of ice lenses in the 1000 cm<sup>3</sup> wedge cutter is due to them representing a much smaller proportion of the sampled volume than the other methods. However, uncertainties in measurements of ice layer densities are poorly constrained. Previous measurements have produced a wide range of densities values, such as 630 to 950 kg m<sup>-3</sup> in the Canadian Arctic (Marsh, 1984) and 400 to 800 kg m<sup>-3</sup> in seasonal snow on the Greenland ice sheet (Pfeffer and Humphrey, 1996). Unfortunately, no ice layer was present in the sample measured by the  $\mu$ CT. The large variability in ice layer density measured by different instruments in this study suggests that this topic needs further investigation towards the development of a more precise measure-

ment technique, especially due to the significance of this measurement for radiative transfer modeling (Durand et al., 2008).

In addition, ice layers evolved during the two field days. On the first day, the ice layers were very heterogeneous and horizontally discontinuous. After that, warm temperatures and melt in the upper most layers lead to more pronounced and continuous ice layers on the second day. The SMP provided evidence for the thickening of the ice layers. To avoid breaking the sensor, the SMP immediately stops measuring once a force threshold of 41 N is reached, which means that the layer is too hard for the instrument to penetrate. The SMP force threshold of 41 N was reached for 31 % (4 out of 13) and 56 % (13 out of 23) of the measurements on the first and second day, respectively.

For the  $\mu$ CT measurements, the blocks were extracted on the first day when ice layers were less pronounced. No ice layers were contained in those blocks, as the  $\mu$ CT data showed no distinct ice layers. Density peaks, however, were found in the lower part of the profile, e.g. at 80 cm snow depth (Fig. 3). These density peaks correspond to melt-freeze crusts consisting of larger aggregated structures.

### 4.2.3 Unresolved variation

The unresolved variation represents the density variation within a layer. This variation is not captured by the measurement methods with coarser vertical resolution and cannot be reconstructed. The relative unresolved variations were up to 7.7 % (for averaging the  $\mu$ CT densities to match the traditional layers), with a standard deviation of 5.0 %, expressed as percentage of the mean  $\mu$ CT density. On average an unresolved density variation of 7.7 % seems tolerable, but it becomes a critical variable, as the loss of small density variations will propagate through all parametrization which are based on density, such as permeability (e.g. Zermatten et al., 2014) or thermal conductivity (e.g. Calonne et al., 2011). Figure 8b illustrates this: the high resolution density profile of  $\mu$ CT sample No. 9 loses all of its detail if measured with the vertical resolution of the box cutter. The temperature gradient inside the snowpack depends on variations of the thermal conductivity caused by variations in density (Kaempfer et al., 2005; Calonne et al., 2011; Riche and Schneebeli, 2013). Losing density

variation means losing local maxima and minima in temperature gradient, and therefore missing the driver for potential weak layer formation. Köchle and Schneebeli (2014) also mentioned the limited resolution of a traditional snow profile as a major drawback for the characterization of weak layers. Density variations are known to have a large influence on mechanical properties (Schweizer et al., 2011) and in addition on microwave signatures as they act as interfaces for wave reflection (Wiesmann and Mätzler, 1999).

## 5 Conclusions

This paper compared the snow densities measured by different methods during the MicroSnow Davos 2014 workshop. In general, the agreement between density cutters and  $\mu$ CT measurements was 5 to 9 %, with a bias of  $-5$  to  $2$  %, expressed as percentage of the mean  $\mu$ CT density. Box cutter and  $\mu$ CT measurements in the lab agreed within 8 %, where the box cutter showed a slight overestimation of 5 % (Fig. 2, Table 4). In the field, the density cutters tended to overestimate low densities (1 to 6 %) and underestimate high densities (1 to 6 %) with respect to the  $\mu$ CT densities, with a threshold for over- and underestimation of 296 and 350 kg m<sup>-3</sup> depending on the cutter type (Fig. 4, Table 5). Using the mean of all measurement methods applied in the field ( $\mu$ CT, box, wedge and cylinder cutter) and ignoring ice layers, the variation of layer density between the methods was 2 to 5 % with a bias of  $-1$  to  $1$  %, expressed as percentage of the mean layer density (Fig. 5, Table 6). These results are also encouraging for applications where a coarse vertical resolution is sufficient (i.e. microwave snow modeling). For coarse resolutions, the technically simple cutters provide the same information as the more time consuming and cost intensive  $\mu$ CT. However, our results are valid if ice layers were not considered, as the methods differed significantly in their ability to resolve the density of thin ice layers. Due to calibration issues, the density derived from the SnowMicroPen (SMP) had to be discarded for now from the intercomparison.

The density profiles revealed by the measurement methods differed considerably (Fig. 8). Traditional layers are defined by an observer with respect to changes in snow properties,

whereas the  $\mu$ CT provides a much higher vertical resolution. In particular the millimeter scale density variations revealed by the  $\mu$ CT contrasted the thick layers with sharp boundaries introduced by the observer. This leads to much higher resolved density profiles to initiate or validate snow cover and microwave models. In this regard, the unresolved variation (Fig. 7), i.e. the density variation within a layer lost during the aggregation into thicker layers or during sampling with coarse vertical resolution, is a critical variable, as density variations are of key importance for snow metamorphism, snowpack stability or scattering of electromagnetic waves. In general, our results suggest that snow densities measured by different methods agree within 9 %.

*Acknowledgements.* The authors want to thank all MicroSnow Davos 2014 organizers and instrument operators. M. Proksch was supported by ESA's Networking/Partnering Initiative NPI No. 235-2012.

## References

Adams, E. and Sato, A.: Model of effective thermal conductivity of a dry snow cover composed of uniform spheres, *Annals of Glaciology*, 18, 300–304, 1993.

Albert, M.: Modeling heat, mass, and species transport in polar firn, *Annals of Glaciology*, 23, 138 – 143, 1996.

Brun, E., Martin, E., Simon, V., Gendre, C., and Coleou, C.: An energy and mass model of snow cover suitable for operational avalanche forecasting, *Journal of Glaciology*, 35, 333–342, 1989.

Calonne, N., Flin, F., Morin, S., Lesaffre, B., Rolland du Roscoat, S., and Geindreau, C.: Numerical and experimental investigations of the effective thermal conductivity of snow, *Geophysical Research Letters*, 38, L23 501, doi:10.1029/2011GL049234, 2011.

Calonne, N., Geindreau, C., Flin, F., Morin, S., Lesaffre, B., Rolland du Roscoat, S., and Charrier, P.: 3-D image-based numerical computations of snow permeability: links to specific surface area, density, and microstructural anisotropy, *The Cryosphere*, 6, 939–951, doi:10.5194/tc-6-939-2012, 2012.

Carroll, T.: A comparison of the CRREL 500 cm<sup>3</sup> tube and the ILTS 200 and 100 cm<sup>3</sup> box cutters used for determining snow densities, *Journal of Glaciology*, 18, 334 – 337, 1977.

- Conger, S. M. and McClung, D.: Instruments and Methods: Comparison of density cutters for snow profile observations, *Journal of Glaciology*, 55, 163–169, doi:10.3189/002214309788609038, 2009.
- Denoth, A., Foglar, A., Weiland, P., Mätzler, C., and Aebischer, H.: A comparative study of instruments for measuring the liquid water content of snow, *Journal of Applied Physics*, 56, 2154 – 2160, doi:10.1063/1.334215, 1984.
- Derksen, C. and Brown, R.: Spring snow cover extent reductions in the 2008 – 2012 period exceeding climate model projections, *Geophysical Research Letters*, 39, L19504, doi:10.1029/2012GL053387, 2012.
- Domine, F., Taillandier, A., and Simpson, W. R.: A parameterization of the specific surface area of seasonal snow for field use and for models of snowpack evolution, *Journal of Geophysical Research: Earth Surface*, 112, F02031, doi:10.1029/2006JF000512, 2007.
- Domine, F., Albert, M., Huthwelker, T., Jacobi, H.-W., Kokhanovsky, A. A., Lehning, M., Picard, G., and Simpson, W. R.: Snow physics as relevant to snow photochemistry, *Atmospheric Chemistry and Physics*, 8, 171–208, doi:10.5194/acp-8-171-2008, 2008.
- Durand, M., Kim, E., and Margulis, S. A.: Quantifying Uncertainty in Modeling Snow Microwave Radiance for a Mountain Snowpack at the Point-Scale, Including Stratigraphic Effects, *IEEE Transactions on Geoscience and Remote Sensing*, 46, 1753 – 1767, doi:10.1109/TGRS.2008.916221, 2008.
- Durand, M., Kim, E. J., Margulis, S. A., and Molotch, N.: A first-order characterization of errors from neglecting stratigraphy in forward and inverse passive microwave modeling of snow, *IEEE Geoscience and Remote Sensing Letters*, 8, 730–734, doi:10.1109/LGRS.2011.2105243, 2011.
- Fierz, C., Armstrong, R., Durand, Y., Etchevers, P., Greene, E., McClung, D., Nishimura, K., Satyawali, P., and Sokratov, S. A.: The international classification for seasonal snow on the ground, HP-VII Technical Documents in Hydrology N°83, IACS Contribution N°1, UNESCO-IHP, Paris., 2009.
- Flanner, M. and Zender, C.: Linking snowpack microphysics and albedo evolution, *Journal of Geophysical Research*, 111, D12208, doi:10.1029/2005JD006834, 2006.
- Freitag, J., Wilhelms, F., and Kipfstuhl, S.: Microstructure-dependent densification of polar firn derived from X-ray microtomography, *Journal of Glaciology*, 50, 243–250, doi:10.3189/172756504781830123, 2004.

- Gergely, M., Schneebeli, M., and Roth, K.: First experiments to determine snow density from diffuse near-infrared transmittance, *Cold Regions Science and Technology*, 64, 81–86, doi:10.1016/j.coldregions.2010.06.005, 2010.
- 5 Hagenmuller, P., Chambon, G., Lesaffre, B., Flin, F., and Naaïm, M.: Energy-based binary segmentation of snow microtomographic images, *Journal of Glaciology*, 59, 859–873, doi:10.3189/2013JoG13J035, 2013.
- Harper, J. T. and Bradford, J. H.: Snow stratigraphy over a uniform depositional surface: spatial variability and measurement tools, *Cold Regions Science and Technology*, 37, 289 – 298, doi:10.1016/S0165-232X(03)00071-5, 2003.
- 10 Hawley, R. L., Brandt, O., Morris, E. M., Kohler, J., Shepherd, A. P., and Wingham, D. J.: Instruments and Methods: Techniques for measuring high-resolution firn density profiles: case study from Kongsvegen, Svalbard, *Journal of Glaciology*, 54, 463–468, doi:10.3189/002214308785837020, 2008.
- Jordan, R.: A one-dimensional temperature model for a snow cover, Technical Documentation for SNTHERM 89, Tech. rep., CRREL special report 91–16, U.S. Army Corps of Engineers, Hanover, NH, USA, 64, 1991.
- 15 Kaempfer, T. U. and Schneebeli, M.: Observation of isothermal metamorphism of new snow and interpretation as a sintering process, *Journal of Geophysical Research*, 112, D24 101, doi:10.1029/2007JD009047, 2007.
- 20 Kaempfer, T. U., Schneebeli, M., and Sokratov, S. A.: A microstructural approach to model heat transfer in snow, *Geophysical Research Letters*, 32, 1–5, doi:10.1029/2005GL023873, 2005.
- Kane, H.: A neutron probe for the determination of snow density and its use in Antarctica, Tech. rep., Institute of polar studies report No 28, Ohio State University, Research Foundation Columbus, Ohio 43212, 1969.
- 25 Kawamura, T.: Nondestructive, three-dimensional density measurements of ice core samples by X ray computed tomography, *Journal of Geophysical Research: Solid Earth*, 95, 12 407–12 412, doi:10.1029/JB095iB08p12407, 1990.
- Kendra, J., Ulaby, F., and Sarabandi, K.: Snow probe for in situ determination of wetness and density, *Geoscience and Remote Sensing, IEEE Transactions on*, 32, 1152–1159, doi:10.1109/36.338363, 1994.
- 30 Kerbrat, M., Pinzer, B., Huthwelker, T., Gäggeler, H. W., Ammann, M., and Schneebeli, M.: Measuring the specific surface area of snow with X-ray tomography and gas adsorption: comparison

and implications for surface smoothness, *Atmospheric Chemistry and Physics*, 8, 1261–1275, doi:10.5194/acp-8-1261-2008, 2008.

Köchle, B. and Schneebeli, M.: 3D microstructure and numerical calculation of elastic properties of alpine snow with focus on weak layers, *Journal of Glaciology*, 60, 1–20, 2014.

5 Kokhanovsky, A. A. and Zege, E.: Scattering optics of snow, *Applied Optics*, 43, 1589 – 1602, 2004.

Lehning, M., Bartelt, P., Brown, B., Fierz, C., and Satyawali, P. K.: A physical SNOWPACK model for the Swiss avalanche warning Part II. Snow microstructure, *Cold Regions Science and Technology*, 35, 147–167, doi:10.1016/S0165-232X(02)00073-3, 2002.

10 Lenaerts, J. T. M., van den Broeke, M. R., Déry, S. J., van Meijgaard, E., van de Berg, W. J., Palm, S. P., and Sanz Rodrigo, J.: Modeling drifting snow in Antarctica with a regional climate model: 1. Methods and model evaluation, *Journal of Geophysical Research: Atmospheres*, 117, D05 108, doi:10.1029/2011JD016145, 2012.

Löwe, H., Riche, F., and Schneebeli, M.: A general treatment of snow microstructure exemplified by an improved relation for thermal conductivity, *The Cryosphere*, 7, 1473–1480, doi:10.5194/tc-7-1473-2013, 2013.

15 Lundy, C. C., Edens, M. Q., and Brown, R. L.: Measurement of snow density and microstructure using computed tomography, *Journal of Glaciology*, 48, 312–316, doi:10.3189/172756502781831485, 2002.

20 Marsh, P.: Wetting front advance and freezing of meltwater within a snow cover: 1. Observations in the Canadian Arctic, *Water Resources Research*, 20, 1853–1864, 1984.

Matzl, M. and Schneebeli, M.: Stereological measurement of the specific surface area of seasonal snow types: Comparison to other methods, and implications for mm-scale vertical profiling, *Cold Regions Science and Technology*, 64, 1–8, doi:10.1016/j.coldregions.2010.06.006, 2010.

25 Mätzler, C.: Microwave permittivity of dry snow, *IEEE Transactions on Geoscience and Remote Sensing*, 34, 573–581, doi:10.1109/36.485133, 1996.

Monti, F., Cagnati, A., Valt, M., and Schweizer, J.: A new method for visualizing snow stability profiles, *Cold Regions Science and Technology*, 78, 64 – 72, doi:10.1016/j.coldregions.2012.02.005, 2012.

30 Morris, E. M. and Cooper, J. D.: Instruments and Methods Density measurements in ice boreholes using neutron scattering, *Journal of Glaciology*, 49, 599–604, doi:10.3189/172756503781830403, 2003.


Neumann, T. and Waddington, E.: Effects of firn ventilation on isotopic exchange, *Journal of Glaciology*, 50, 183 – 194, 2004.



- Pfeffer, W. and Humphrey, N.: Determination of timing and location of water movement and ice-layer formation by temperature measurements in sub-freezing snow, *Journal of Glaciology*, 42, 292 – 304, 1996.
- Proksch, M., Löwe, H., and Schneebeli, M.: Density, specific surface area and correlation length of snow measured by high-resolution penetrometry, *Journal of Geophysical Research: Earth Surface*, 120, 346–362, doi:10.1002/2014JF003266, 2015.
- Pulliainen, J. and Hallikainen, M.: Retrieval of regional snow water equivalent from space-borne passive microwave observations, *Remote Sensing of Environment*, 75, 76 – 85, 2001.
- Reuter, B., Schweizer, J., and van Herwijnen, A.: A process-based approach to estimate point snow instability, *The Cryosphere*, 9, 837–847, doi:10.5194/tc-9-837-2015, 2015.
- Riche, F. and Schneebeli, M.: Thermal conductivity of snow measured by three independent methods and anisotropy considerations, *The Cryosphere*, 7, 217–227, doi:10.5194/tc-7-217-2013, 2013.
- Rutter, N., Sandells, M., Derksen, C., Toose, P., Royer, A., Montpetit, B., Langlois, A., Lemmetyinen, J., and Pulliainen, J.: Snowstratigraphic heterogeneity within ground-based passive microwave radiometer footprints: Implications for emission modeling, *Journal of Geophysical Research: Earth Surface*, 119, 550–565, doi:10.1002/2013JF003017, 2014.
- Scapozza, C. and Bartelt, P. A.: The influence of temperature on the small-strain viscous deformation mechanics of snow: a comparison with polycrystalline ice, *Annals of Glaciology*, 37, 90–96, doi:10.3189/172756403781815410, 2003.
- Schneebeli, M. and Johnson, J.: A constant-speed penetrometer for high-resolution snow stratigraphy, *Annals of Glaciology*, 26, 107–111, 1998.
- Schneebeli, M. and Sokratov, S.: Tomography of temperature gradient metamorphism of snow and associated changes in heat conductivity, *Hydrological Processes*, 18, 3655–3665, doi:10.1002/hyp.5800, 2004.
- Schweizer, J., van Herwijnen, A., and Reuter, B.: Measurements of weak layer fracture energy, *Cold Regions Science and Technology*, 69, 139 – 144, doi:10.1016/j.coldregions.2011.06.004, 2011.
- Shimizu, H.: Air permeability of deposited snow, *Contributions from the Institute of Low Temperature Science*, A22, 1–32, <http://eprints.lib.hokudai.ac.jp/dspace/handle/2115/20234>, 1970.
- Sturm, M., Holmgren, J., König, M., and Morris, K.: The thermal conductivity of seasonal snow, *Journal of Glaciology*, 43, 26–41, 1997.

- Tiuri, M. and Sihvola, A.: Snow fork for field determination of the density and wetness profiles of a snow pack, in: Hydrologic Applications of Space Technology (Proceedings of the Cocoa Beach Workshop, Florida, August 1985). IAHS Publ. no. 160, pp. 225 –230, 1986.
- 5 Tiuri, M., Sihvola, A., Nyfors, E., and Hallikainen, M.: The Complex Dielectric Constant of Snow at Microwave Frequencies, *IEEE Journal of Oceanic Engineering*, 9, 377 – 382, 1984.
- Torquato, S.: *Random Heterogeneous Materials*, Springer, New York, 2002.
- Town, M., Warren, S., Walden, V., and Waddington, E.: Effect of atmospheric water vapor on modification of stable isotopes in near-surface snow on ice sheets, *Journal of Geophysical Research*, 113, D24 303, doi:10.1029/2008JD009852, 2008.
- 10 Wang, X. and Baker, I.: Observation of the microstructural evolution of snow under uniaxial compression using X-ray computed microtomography, *Journal of Geophysical Research: Atmospheres*, 118, 12,371–12,382, doi:10.1002/2013JD020352, 2013JD020352, 2013.
- Wiesmann, A. and Mätzler, C.: Microwave emission model of layered snowpacks, *Remote Sensing of Environment*, 70, 307–316, doi:10.1016/S0034-4257(99)00046-2, 1999.
- 15 Zermatten, E., Schneebeli, M., Arakawa, H., and Steinfeld, A.: Tomography-based determination of porosity, specific area and permeability of snow and comparison with measurements, *Cold Regions Science and Technology*, 97, 33 – 40, doi:10.1016/j.coldregions.2013.09.013, 2014.

**Table 1.** Vertical resolution and measurement volume of the different methods. Measurement time in the field is per meter snow depth and includes digging of a snow pit, if necessary.

Method	Vertical resolution (mm)	Volume (cm <sup>3</sup> )	Measurement time field	Post processing	Cost/instrument (Euro)
$\mu$ CT	0.018	0.1	1 h	1 h–1 week	300 k
Wedge cutter	100 <sup>a</sup>	1000	1 h	–	50
Box cutter	30 <sup>a</sup>	100	1.5 h	–	50
Cylinder cutter	37  2.0 <sup>a</sup>	100	1.5 h	15 min <sup>b</sup>	50

<sup>a</sup> Enhanced/reduced by letting samples overlap or spacing them, Sect. 2.1.

<sup>b</sup> If measurements are taken per layer, Sect. 2.1.

**Table 2.** Depth below surface and number of measurements/samples per block for the instruments used in the lab.

Method	Depth below surface (cm)	Number of samples per block
$\mu$ CT	2.9–6.8	2
Box cutter	0–bottom	2–8

**Table 3.** Date of measurement and number of measurements/samples for the instruments used in the field.

Method	Date	Number of measurements/samples
$\mu$ CT	11 Mar 2014	18 samples
Box cutter	12 Mar 2014	44 samples
Wedge cutter	11 Mar 2014	28 samples
Cylinder cutter	11 Mar 2014	15 samples

**Table 4.** Statistics for the comparison of cutter and  $\mu$ CT measurements in the lab (Fig. 2) and in the field (Fig. 4). Bias/RMSE are expressed in % of the mean  $\mu$ CT density. Significant agreement ( $p$  val < 0.01) is indicated by bold numbers.

Instrument	Lab			Field		
	Bias (%)	RMSE (%)	$R^2$ (-)	Bias (%)	RMSE (%)	$R^2$ (-)
Box cutter	-5	8	<b>0.90</b>	-1	7	<b>0.90</b>
Wedge cutter				2	9	<b>0.93</b>
Cylinder cutter				-1	5	<b>0.95</b>

**Table 5.** Slope, intercept and  $R^2$  for the linear fit of the cutter densities to the  $\mu$ CT densities averaged to the resolutions of the respective cutter shown in Fig. 4. Significance ( $p$  val  $< 0.01$ ) for the slope and the intercept is indicated by bold numbers.

Instrument	Slope (–)	Intercept ( $\text{kg m}^{-3}$ )	$R^2$ (–)	threshold over-/ underestimation ( $\text{kg m}^{-3}$ )	overestimation low densities (%)	underestimation high densities (%)
Box cutter	<b>0.79</b>	<b>71</b>	0.89	350	4	2
Wedge cutter	<b>0.66</b>	<b>106</b>	0.93	310	6	6
Cylinder cutter	0.90	<b>31</b>	0.95	296	1	1

**Table 6.** Statistics for the comparison of the field measurements to the mean layer densities (Fig. 5), expressed in % of the mean layer densities. Significant agreement ( $p$  val  $< 0.01$ ) is indicated by bold numbers.

Instrument	No ice layers			With ice layers		
	Bias (%)	RMSE (%)	$R^2$ (-)	Bias (%)	RMSE (%)	$R^2$ (-)
$\mu$ CT	-1	4	<b>0.99</b>	-10	18	0.44
Box cutter	1	2	<b>0.99</b>	7	12	<b>0.76</b>
Wedge cutter	1	5	<b>0.99</b>	-9	20	0.24
Cylinder cutter	-1	3	<b>0.99</b>	12	35	<b>0.71</b>



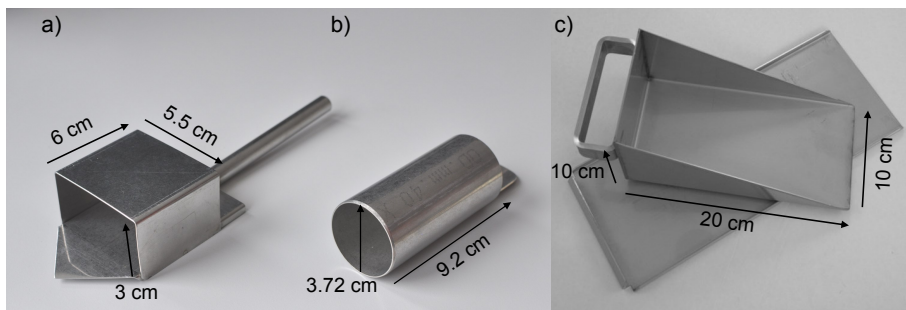


**Figure 1.** Density cutters used at the MicroSnow workshop: (a) box, (b) cylinder, and (c) wedge (from <http://snowmetrics.com/shop/rip-1-cutter-1000-cc/>).

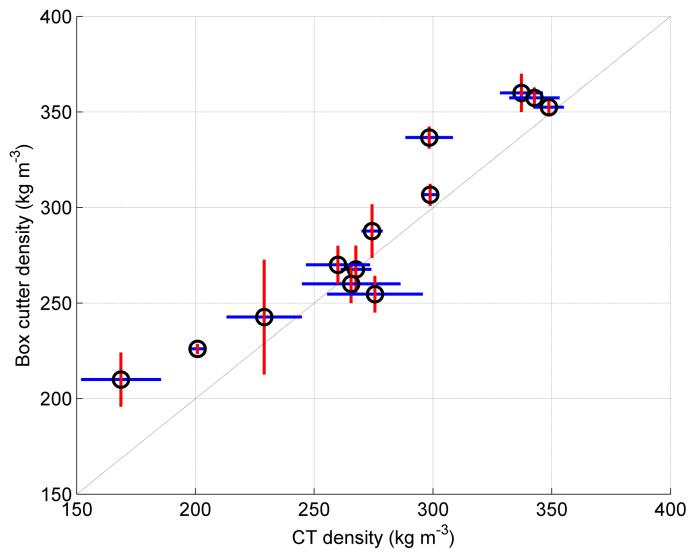


**Figure 2** The top three cutter measurements (0–9 cm) in each of 13 blocks were averaged to best match the location of the  $\mu$ CT samples. Error bars are  $\pm$  one standard deviation, resulting from these three cutter measurements (red) and the three  $\mu$ CT samples per block (blue).

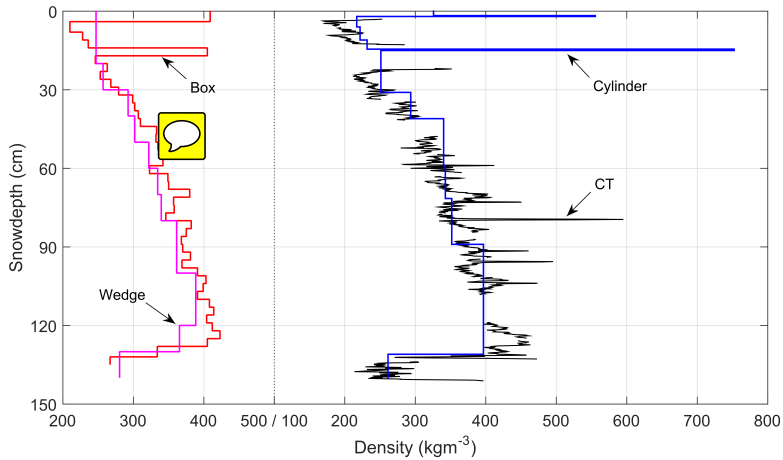


**Figure 3.** Density profile measured by different methods. Two methods each are displayed separately for better visibility. Note that the cylinder profile shows the density with respect to the stratigraphic layers.

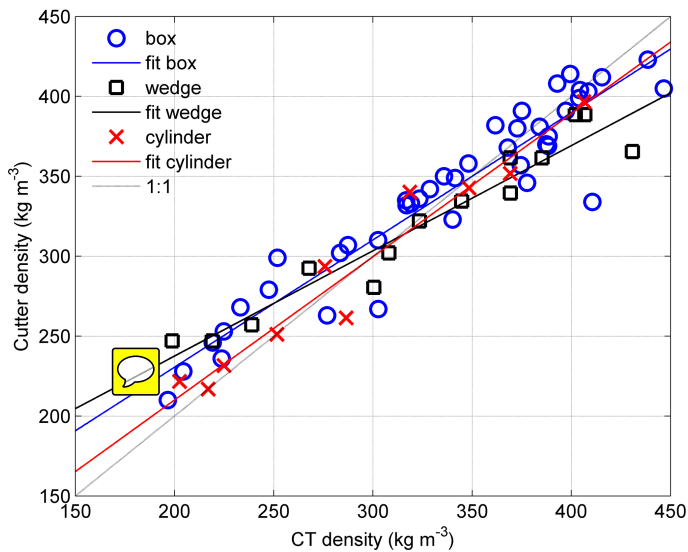


**Figure 4.** Cutter density vs.  $\mu\text{CT}$  density averaged to the resolution of the cutters (symbols). In addition a linear fit for each comparison is shown (lines). Fit statistics are given in Table 5.

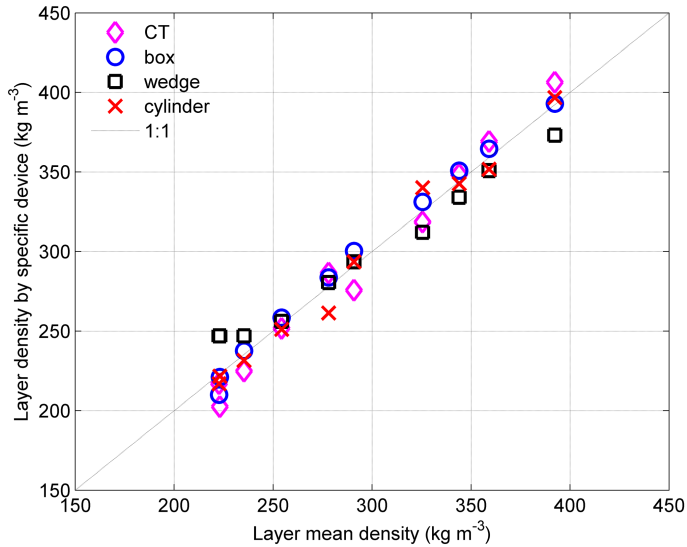


**Figure 5.** Different measurement methods averaged to match the traditional layers, vs. the mean layer density. Mean layer densities are the average of all layer densities of the different methods. Statistics are given in Table 6.

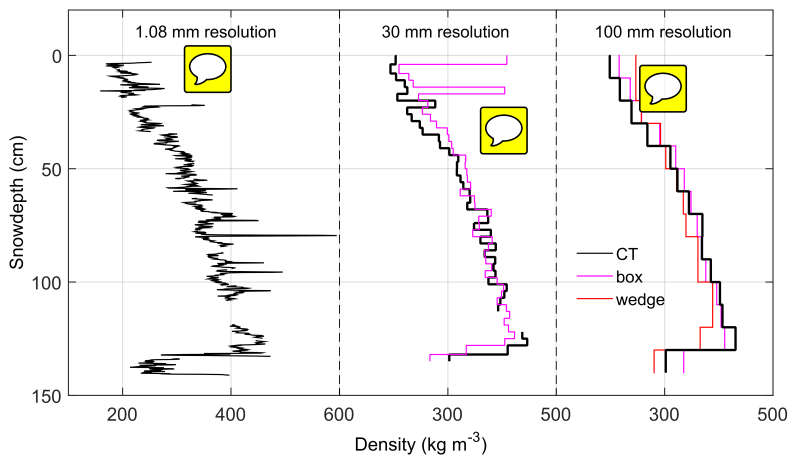


**Figure 6.**  $\mu$ CT derived density (black), subsequently averaged to 30 mm (black, middle) and 100 mm (black, right) vertical resolution. For comparison, the box cutter densities are shown in raw resolution (magenta, middle) and averaged to 100 mm resolution (magenta, right). The wedge cutter density is as well shown in raw resolution (red, right).

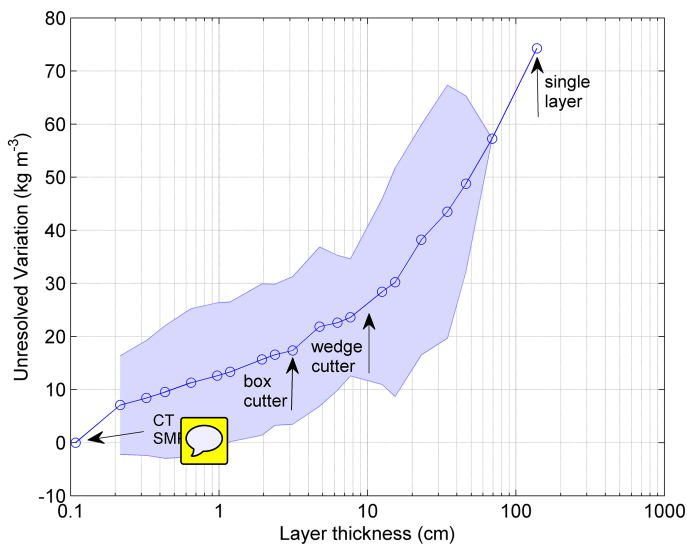


**Figure 7.** Unresolved variation of  $\mu\text{CT}$  profile vertically averaged to larger layer thickness, with the vertical resolution of box cutter (3 cm), wedge cutter (10 cm) and a single layer profile indicated. The shaded area indicates  $\pm$  one standard deviation.

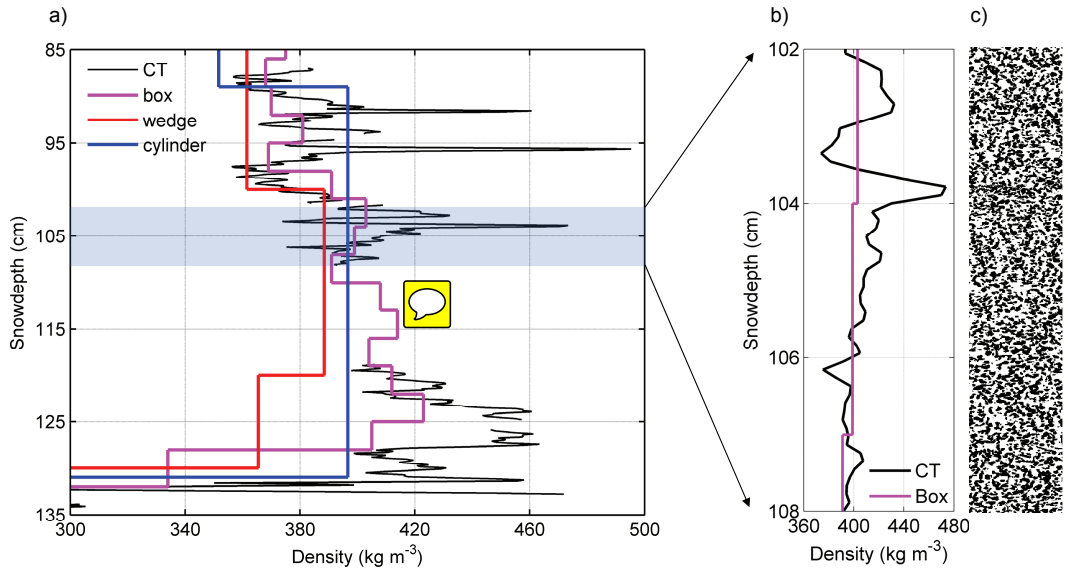


**Figure 8.** Close-up of the lower part of the density profile measured by the density cutters and  $\mu\text{CT}$  (a). The shaded area indicates the location of the  $\mu\text{CT}$  sample No. 9. Density profile (b) and 2-D reconstruction (c) of  $\mu\text{CT}$  sample No. 9.